

Photoproduction of Baryons Decaying into $N\pi$ and $N\eta$

A.V. Anisovich^{1,2}, A. Sarantsev^{1,2}, O. Bartholomy¹, E. Klempt¹, V.A. Nikonov^{1,2}, and U. Thoma^{1,3}

¹ Helmholtz–Institut für Strahlen– und Kernphysik, Universität Bonn, Germany

² Nuclear Physics Institute, Gatchina, Russia

³ Physikalisches Institut, Universität Gießen, Germany

Received: November 10, 2018/ Revised version:

Abstract. A combined analysis of photoproduction data on $\gamma p \rightarrow \pi N$, ηN was performed including the data on $K\Lambda$ and $K\Sigma$. The data are interpreted in an isobar model with s -channel baryon resonances and π , $\rho(\omega)$, K , and K^* exchange in the t -channel. Three baryon resonances have a substantial coupling to ηN , the well known $N(1535)S_{11}$, $N(1720)P_{13}$, and $N(2070)D_{15}$. The inclusion of data with open strangeness reveals the presence of further new resonances, $N(1840)P_{11}$, $N(1875)D_{13}$ and $N(2170)D_{13}$.

PACS: 11.80.Et, 11.80.Gw, 13.30.-a, 13.30.Ce, 13.30.Eg, 13.60.Le 14.20.Gk

1 Introduction

The energy levels of bound systems and their decay properties provide valuable information about the constituents and their interactions [1]. In quark models, the dynamics of the three constituent quarks in baryons support a rich spectrum, much richer than the energy scheme experiments have established so far [2, 3, 4]. This open issue is referred to as the problem of missing resonances. The intense discussion of the exotic baryon resonance $\Theta^+(1540)$ [5, 6, 7], of its existence and of its interpretation, has shown limits of the quark model and underlined the need for a deeper understanding of baryon spectroscopy. Here, the study of pentaquarks has played a pioneering role, but any new model has to be tested against the excitation spectrum of the nucleon as well. The properties of baryon resonances are presently under intense investigations at several facilities like ELSA (Bonn), GRAAL (Grenoble), JLab (Newport News), MAMI (Mainz), and Spring-8 (Hyogo). The aim is to identify the resonance spectrum, to determine spins, parities, and decay branching ratios and thus to provide constraints for models.

The largest part of our knowledge on baryons stems from pion induced reactions. In elastic πN scattering, the unitarity condition provides strong constraints for amplitudes close to the unitarity limit, since production couplings are related directly to the widths of resonances and to the cross section. If a resonance has however a large inelasticity, its production cross section in πN scattering is small and it contributes only weakly to the final state. Thus resonances may conceal themselves from observation in elastic scattering. This effect could be a reason why the number of observed states is much smaller than

predicted by quark models [2, 3, 4]. Information on resonances coupled weakly to the πN channel can be obtained from photoproduction experiments and the study of final states different from πN such as multibody final states or final states containing open strangeness.

The information from photoproduction experiments is complementary to experiments with hadronic beams and gives access to additional properties like helicity amplitudes. Experiments with polarised photons provide information which may be very sensitive to resonances having a small cross section. A clear example of such an effect is the observation of the $N(1520)D_{13}$ resonance in η photoproduction. It contributes very little to the unpolarised cross section but its interference with $N(1535)S_{11}$ produces a strong effect in the beam asymmetry. Photoproduction can also provide a very strong selection tool: combining a circularly polarised photon beam and a longitudinally polarised target provides a tool to select states with helicity $1/2$ or $3/2$ depending on whether the target polarisation is parallel or antiparallel to the photon helicity.

Baryon resonances have large, overlapping widths rendering difficult the study of individual states, in particular of those only weakly excited. This problem can be overcome partly by looking at specific decay channels. The η meson for example has isospin $I = 0$ and consequently, the $N\eta$ final state can only be reached via formation of N^* resonances. Then even a small coupling of a resonance to $N\eta$ identifies it as N^* state. A key point in the identification of new baryon resonances is the combined analysis of data on photo- (and pion-) induced reactions with different final states. Resonances must have the same masses, total widths, and gamma-nucleon couplings, in all reactions under study. This imposes strong constraints for the analysis.

In the present paper we report results of a combined analysis of photoproduction experiments with πN , ηN , $K\Lambda$, and $K\Sigma$ final states. This work is a first step of a forthcoming analysis of all reactions with production of baryon resonances in the intermediate state. This paper concentrates on the reactions $\gamma p \rightarrow N\pi$ and $N\eta$, including available polarisation measurements. Results on photoproduction of open strangeness are presented in a subsequent paper [8].

The outline of the paper is as follows: The fit method is described in section 2, data and fit are compared in section 3. In section 4 we present the main results of this analysis and discuss the statistical significance of new baryon resonances. Interpretations are offered for the newly found resonances. The paper ends with a short summary in section 5.

2 Fit method

2.1 Analytical properties of the amplitude and resonance–Reggeon duality

The choice of amplitudes used to describe the data is partly driven by experimental observations. In pion photoproduction, angular distributions exhibit strong variations indicating the presence of baryon resonances. On the other hand, all data on single-meson photoproduction have prominent forward peaks in the region above 2000 MeV which can be associated with t -channel exchange processes. Regge behaviour, extrapolated to the low-energy region, describes the cross section in the resonance region “on average”. This feature is known as Reggeon–resonance duality (see [9] and references therein). It gave hope for a self-consistent construction of hadron–hadron interactions in both, the low-energy and the high-energy region. However there is a problem with unitarity: The s -channel unitarity corrections destroy the one-Reggeon exchange picture, while the s -channel resonance amplitudes do not satisfy the t -, u -channel unitarity [10]. So it seems reasonable to extract the resonance structure of the amplitude together with phenomenological reggeized t - and u -channel exchange amplitudes.

The scattering amplitude has the following analytical properties. The partial-wave or multipole amplitudes contain singularities when the scattering particles can form a bound state with mass M . Unstable bound states with a finite width Γ have a pole singularity at $s = M^2 - i\Gamma M$ in the complex plane. At the opening of thresholds, the amplitude acquires a square root singularity (right-hand singularity); t -exchange leads to left-hand singularities at $t = \mu^2$ (one-particle exchange with mass μ), $t = 4\mu^2$ (exchange of two of these particles) and so on. In three-body interactions the three-particle rescattering amplitude gives a triangle singularity which may contribute significantly to the cross section under some particular kinematical conditions [11]. Triangle singularities grow logarithmically and are thus weaker than a pole or a threshold singularity. In most cases, triangle singularities can be accounted for by introducing phases to resonance couplings.

In our present analysis, the primary goal is to get information about the leading (pole) singularities of the photoproduction amplitude. For this purpose, a representation of the amplitude as a sum of s -channel resonances together with some t - and u -exchange diagrams is an appropriate representation. Strongly overlapping resonances are parameterised as K -matrix. In many cases it is sufficient to use a relativistic Breit–Wigner parameterisation, though.

We emphasise that the amplitudes given below satisfy gauge invariance, analyticity and unitarity. However, when t -, u -, and s -channel amplitudes are added, unitarity is violated. In principle, this can be avoided by projecting the t - and u -channel amplitudes onto s -channel amplitudes of defined spins and parities. The projected amplitudes are however small, and the violation of unitarity is mild as long as t - and u -channel amplitudes contribute only a small fraction to the total cross section. In this analysis, amplitudes for photoproduction of baryon resonances and their decays are calculated in the framework of relativistic tensor operators. The formalism is fully described in [12]; here parameterisations of resonances used under different conditions are given.

2.2 Parameterisations of resonances

The differential cross section for production of two or more particles has the form:

$$d\sigma = \frac{(2\pi)^4 |A|^2}{4 \sqrt{(k_1 k_2)^2 - m_1^2 m_2^2}} d\Phi_n(k_1 + k_2, q_1, \dots, q_n) \quad (1)$$

where k_i and m_i are the four-momenta and masses of the initial particles (nucleon and γ in the case of photoproduction) and q_i are the four-momenta of final state particles. $d\Phi_n(k_1 + k_2, q_1, \dots, q_n)$ is the n -body phase volume

$$d\Phi_n(k_1 + k_2, q_1, \dots, q_n) = \delta^4(k_1 + k_2 - \sum_{i=1}^n q_i) \prod_{i=1}^n \frac{d^3 q_i}{(2\pi)^3 2q_{0i}} \quad (2)$$

where q_{0i} is time component (energy). The differential cross section for photoproduction of single mesons is given by

$$d\sigma = \frac{\sqrt{(s - (m_\mu + m_B)^2)(s - (m_\mu - m_B)^2)}}{16\pi s(s - m_N^2)} |A|^2 \quad (3)$$

where $s = (k_1 + k_2)^2 = (q_1 + q_2)^2$ is the square of the total energy, m_μ , ($\mu = \pi, \eta, K$), m_B ($B = N, \Lambda, \Sigma$) the meson and baryon masses, respectively.

The η photoproduction cross section is dominated by $N(1535)S_{11}$. It overlaps with $N(1650)S_{11}$ and the two S_{11} resonances are described as two-pole, four-channel K -matrix (πN , ηN , $K\Lambda$ and $K\Sigma$). The photoproduction amplitude can be written in the P -vector approach since the

γN couplings are weak and do not contribute to rescattering. The amplitude is then given by

$$A_a = \hat{P}_b (\hat{I} - i\hat{\rho}\hat{K})_{ba}^{-1}. \quad (4)$$

The phase space $\hat{\rho}$ is a diagonal matrix with

$$\rho_{ab} = \delta_{ab} \rho_a, \quad a, b = \pi N, \eta N, K\Lambda, K\Sigma. \quad (5)$$

and

$$\rho_a(s) = \frac{\sqrt{(s - (m_\mu + m_B)^2)(s - (m_\mu - m_B)^2)}}{s}. \quad (6)$$

The production vector \hat{P} and the K -matrix \hat{K} have the following parameterisation:

$$K_{ab} = \sum_\alpha \frac{g_a^{(\alpha)} g_b^{(\alpha)}}{M_\alpha^2 - s} + f_{ab}, \quad P_b = \sum_\alpha \frac{g_{\gamma N}^{(\alpha)} g_b^{(\alpha)}}{M_\alpha^2 - s} + \tilde{f}_b \quad (7)$$

where M_α , $g_a^{(\alpha)}$ and $g_{\gamma N}^{(\alpha)}$ are the mass, coupling constant and production constant of the resonance α ; f_{ab} and \tilde{f}_b are non-resonant terms.

Other resonances were taken as Breit-Wigner amplitude:

$$A_a = \frac{g_{\gamma N} \tilde{g}_a(s)}{M^2 - s - i M \tilde{\Gamma}_{tot}(s)} \quad (8)$$

States with masses above 1700 MeV were parameterised with a constant width to fit exactly the pole position. For resonances below 1700 MeV, $\tilde{\Gamma}_{tot}(s)$ was parameterised by

$$\tilde{\Gamma}_{tot}(s) = \Gamma_{tot} \frac{\rho_{\pi N}(s) k_{\pi N}^{2L}(s) F^2(L, k_{\pi N}^2(M^2), r)}{\rho_{\pi N}(M^2) k_{\pi N}^{2L}(M^2) F^2(L, k_{\pi N}^2(s), r)}, \quad (9)$$

$$k_a^2(s) = \frac{(s - (m_\mu + m_B)^2)(s - (m_\mu - m_B)^2)}{4s}.$$

Here, L is the orbital momentum and k is the relative momentum for the decay into πN ($\mu = \pi$, $B = N$). $F(L, k^2, r)$ are Blatt-Weiskopf form factors, taken with a radius $r = 0.8$ fm. The exact form of these factors can be found e.g. in [12]. $g_{\gamma N}$ is the production coupling and \tilde{g}_a are decay couplings of the resonance into meson nucleon channels. These couplings are suppressed at large energies by a factor

$$\tilde{g}_a(s) = g_a \sqrt{\frac{1.5 \text{ GeV}^2}{1.0 \text{ GeV}^2 + k_a^2}}. \quad (10)$$

The factor proved to be useful for two-meson photoproduction. For photoproduction of single mesons, it plays almost no role and is only introduced here for the sake of consistency.

The partial widths are related to the couplings as

$$M\Gamma_a = \tilde{g}_a^2 \frac{\rho_a(M^2) k_{\pi N}^{2L}}{F^2(L, k_{\pi N}^2, r)} \frac{m_B + \sqrt{m_B^2 + k_a^2}}{2m_B} \beta_L,$$

$$\beta_L = \frac{1}{L} \prod_{l=1}^L \frac{2l-1}{l}, \quad J = L - \frac{1}{2},$$

$$\beta_L = \frac{1}{2L+1} \prod_{l=1}^L \frac{2l-1}{l}, \quad J = L + \frac{1}{2}. \quad (11)$$

Here J is the total momentum of the state.

2.3 t- and u-channel exchange parameterisations

At high energies, there are clear peaks in the forward direction of photoproduced mesons. The forward peaks are connected with meson exchanges in the t -channel. These contributions are parameterised as π , $\rho(\omega)$, K , and K^* exchanges.

These contributions are reggeized by using [13]

$$T(s, t) = g_1(t) g_2(t) \frac{1 + \xi \exp(-i\pi\alpha(t))}{\sin(\pi\alpha(t))} \left(\frac{\nu}{\nu_0} \right)^{\alpha(t)},$$

$$\nu = \frac{1}{2}(s - u). \quad (12)$$

Here, g_i are vertex functions, $\alpha(t)$ is a function describing the trajectory, ν_0 is a normalisation factor (which can be taken to be 1) and ξ is the signature of the trajectory. Exchanges of π and K have positive, ρ , ω , and K^* exchanges have negative signature.

For $\rho(\omega)$ exchange, $\alpha(t) = 0.50 + 0.85t$. The pion trajectory is given by $\alpha(t) = -0.014 + 0.72t$, the K^* and K trajectories are represented by $\alpha(t) = 0.32 + 0.85t$ and $\alpha(t) = -0.25 + 0.85t$, respectively. The full expression for the t -channel amplitudes can be found in [12].

The u -channel exchanges were parameterised as nucleon, Λ , or Σ exchanges.

3 Fits to the data

In this paper, we report results on baryon resonances and their coupling to $N\pi$ and $N\eta$. The results are based on a coupled-channel analysis of various data sets on photoproduction of different final states. The data comprise CB-ELSA π^0 and η photoproduction data [14, 19], the Mainz-TAPS data [18] on η photoproduction, beam-asymmetry measurements of π^0 and η [15, 16, 20], and data on $\gamma p \rightarrow n\pi^+$ [17]. The high precision data from GRAAL [15] do not cover the low mass region; therefore we extract further data from the compilation of the SAID database [16]. This data allows us to define the ratio of helicity amplitudes for the $\Delta(1232)P_{33}$ resonance.

Data on photoproduction of $K^+\Lambda$, $K^+\Sigma$, and $K^0\Sigma^+$ from SAPHIR [21] and CLAS [22], and beam asymmetry data for $K^+\Lambda$, $K^+\Sigma$ from LEPS [23] are also included in the coupled-channel analysis. The results on couplings of baryon resonances to $K^+\Lambda$ and $K^+\Sigma$ are documented in a separate paper [8].

The fit uses 14 N^* resonances coupling to $N\pi$, $N\eta$, $K\Lambda$, and $K\Sigma$ and 7 Δ resonances coupling to $N\pi$ and

$K\Sigma$. Most resonances are described by relativistic Breit–Wigner amplitudes. For the two S_{11} resonances at 1535 and 1650 MeV, a four-channel K -matrix ($N\pi$, $N\eta$, $K\Lambda$, $K\Sigma$) is used. The background is described by reggeized t -channel π , $\rho(\omega)$, K and K^* exchanges and by baryon exchanges in the s - and u -channels.

The χ^2 values for the final solution of the partial-wave analysis are given in Table 1. Weights are given to the different data sets included in this analysis with which they enter the fits. In the choice of weights, some judgement is needed. The CB-ELSA data on pion and η photoproduction are the main source of the analysis and thus have large weights. The beam polarisation measurements for open strangeness production are also emphasized as discussed in [8]. Fits were performed with a variety of different weights; accepted solutions resulted not only in a good overall χ^2 ; emphasis was laid on having a good fit of all data sets. Changing the weights may result in pictures showing larger discrepancies; the changes of pole positions are only small.

The fit minimises a pseudo-chisquare function which we call χ^2_{tot} . It is given by

$$\chi^2_{\text{tot}} = \frac{\sum w_i \chi_i^2}{\sum w_i N_i} \sum N_i \quad (13)$$

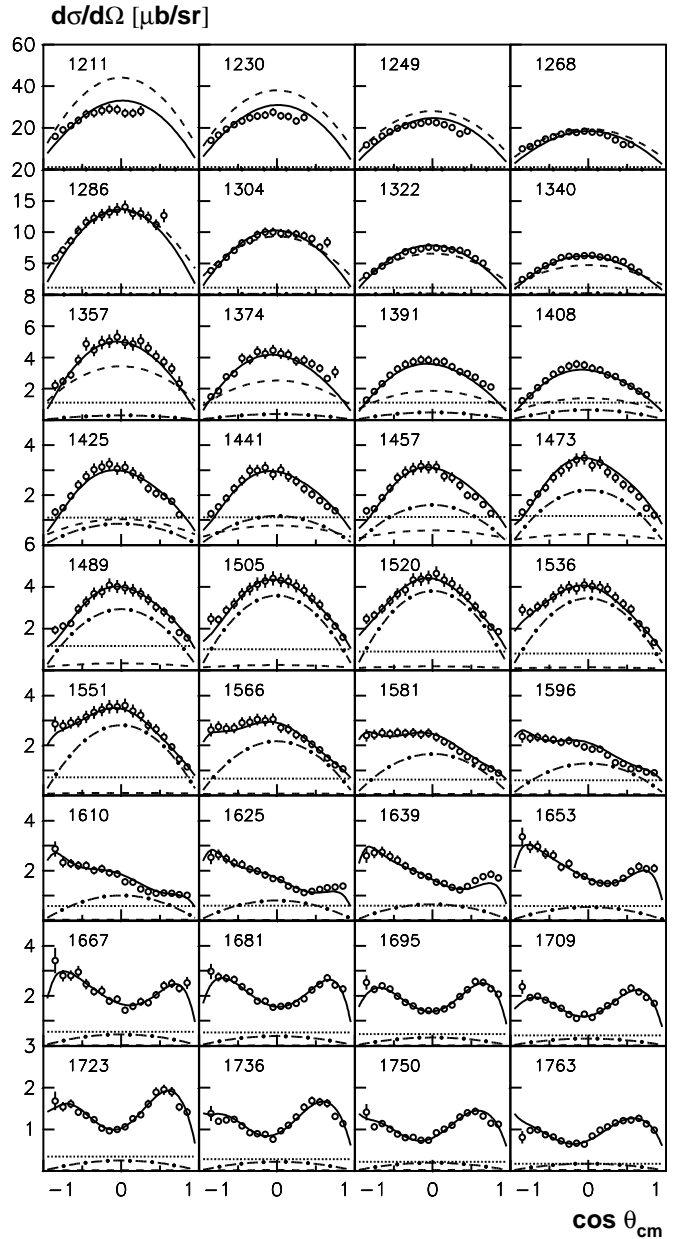
where the N_i are given as N_{data} (per channel) in the 2nd column of Table 1 and the weights in the last column.

Table 1. Data used in the partial wave analysis, χ^2 contributions and fitting weights.

Observable	N_{data}	χ^2	χ^2/N	Weight	Ref.
$\sigma(\gamma p \rightarrow p\pi^0)$	1106	1654	1.50	8	[14]
$\sigma(\gamma p \rightarrow p\pi^0)$	861	2354	2.74	3.5	[15]
$\Sigma(\gamma p \rightarrow p\pi^0)$	469	1606	3.43	2	[15]
$\Sigma(\gamma p \rightarrow p\pi^0)$	593	1702	2.87	2	[16]
$\sigma(\gamma p \rightarrow n\pi^+)$	1583	4524	2.86	1	[17]
$\sigma(\gamma p \rightarrow p\eta)$	100	158	1.60	7	[18]
$\sigma(\gamma p \rightarrow p\eta)$	667	608	0.91	35	[19]
$\Sigma(\gamma p \rightarrow p\eta)$	51	114	2.27	10	[20]
$\Sigma(\gamma p \rightarrow p\eta)$	100	174	1.75	10	[15]
$\sigma(\gamma p \rightarrow \Lambda K^+)$	720	804	1.12	4	[21]
$\sigma(\gamma p \rightarrow \Lambda K^+)$	770	1282	1.67	2	[22]
$P(\gamma p \rightarrow \Lambda K^+)$	202	374	1.85	1	[22]
$\Sigma(\gamma p \rightarrow \Lambda K^+)$	45	62	1.42	15	[23]
$\sigma(\gamma p \rightarrow \Sigma^0 K^+)$	660	834	1.27	1	[21]
$\sigma(\gamma p \rightarrow \Sigma^0 K^+)$	782	2446	3.13	1	[22]
$P(\gamma p \rightarrow \Sigma^0 K^+)$	95	166	1.76	1	[22]
$\Sigma(\gamma p \rightarrow \Sigma^0 K^+)$	45	20	0.46	35	[23]
$\sigma(\gamma p \rightarrow \Sigma^+ K^0)$	48	104	2.20	2	[22]
$\sigma(\gamma p \rightarrow \Sigma^+ K^0)$	120	109	0.91	5	[24]

3.1 Fit to the $p\pi^0$ data

The differential cross sections for the CB-ELSA $\gamma p \rightarrow p\pi^0$ data are shown in Fig. 1. The main fit is represented as solid line. The figure also shows the most important individual contributions. The contribution of $\Delta(1232)$ (given as dashed line, on the left panel) dominates the low-energy region, for small photon energies it even exceeds the experimental cross section, thus underlining the importance of interference effects. Non-resonant background amplitudes, given by a pole at $s \sim -1 \text{ GeV}^2$ and by a u -channel exchange diagram, are needed to describe the shape of the $\Delta(1232)$. The pole at negative s represents the left-hand cuts.



The two S_{11} resonances at 1535 and at 1650 MeV are described as K -matrix. Their sum is depicted as dotted line. The S_{11} contribution is flat in $\cos \Theta_{\text{cm}}$. The contribution of the $D_{13}(1520)$ shown as dash-dotted line in Fig. 1 (left panel). It is strong in the 1400 – 1600 MeV mass region. At higher energies (Fig. 1, right panel) the most significant contributions come from $\Delta(1700)D_{33}$ (dashed line) and from $N(1680)F_{15}$ (dotted line). For invariant $p\gamma$ masses above 1800 MeV, the most forward point in Fig. 1 is not reproduced by the fit. If this point is given a very small error (to ensure that the fit describes these points), the overall agreement between data and fit becomes somewhat worse; resonance masses and widths change by a few MeV, at most.

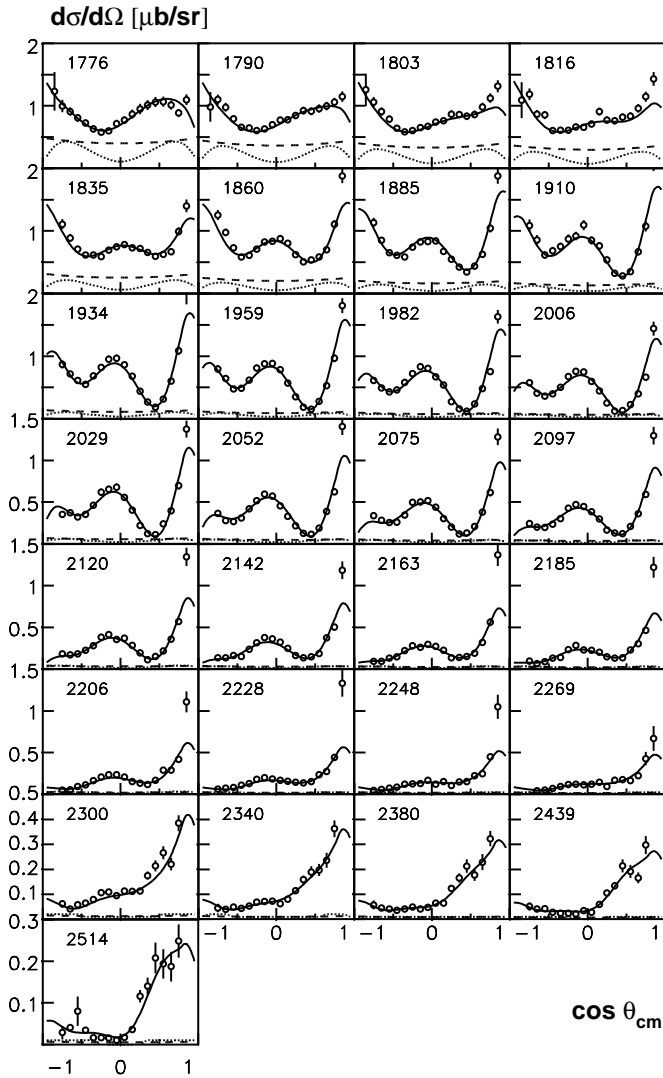


Fig. 1. Differential cross section for $\gamma p \rightarrow p\pi^0$ from CB-ELSA and PWA result (solid line). The left part of the figure shows the contribution of $\Delta(1232)P_{33}$ together with non-resonant background (dashed line), the two S_{11} resonances (dotted line) and $N(1520)D_{13}$ (dash-dotted line); in the right figure, the contributions of $\Delta(1700)D_{33}$ (dashed line) and $N(1680)F_{15}$ (dotted line) are shown.

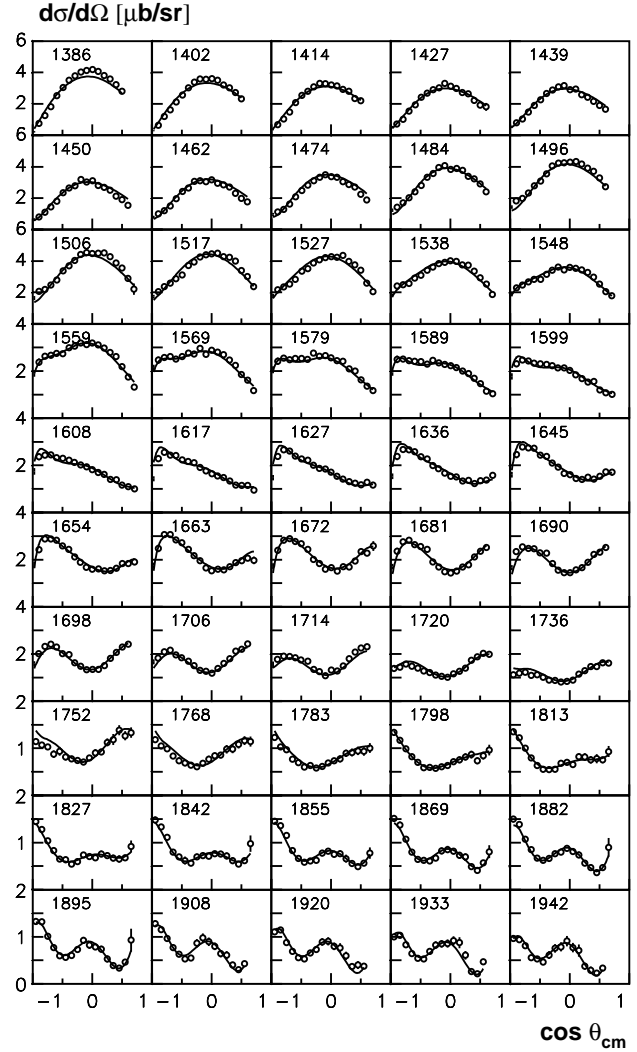


Fig. 2. Differential cross section for $\gamma p \rightarrow p\pi^0$ from GRAAL and PWA result (solid line).

Recent data from GRAAL [15] on the differential cross section for $\gamma p \rightarrow p\pi^0$ and on the photon beam asymmetry Σ are compared to our fit in Figs. 2 and 3; older beam asymmetry data are shown in Fig. 4.

3.2 Fit to $n\pi^+$ photoproduction data

It is important to include data on $n\pi^+$ photoproduction since the combination of the $n\pi^+$ and $p\pi^0$ channels defines the isospin of s -channel baryons. Without this information, pairs of resonances like $N(1700)D_{13}$ and $\Delta(1700)D_{33}$ cannot be separated. A fit with both having large destructively interfering amplitudes may give a good χ^2 even though the fit is physically meaningless. For $\gamma p \rightarrow N^* \rightarrow n\pi^+$ the isotopic coefficient is equal to $\sqrt{2/3}$, for $\gamma p \rightarrow N^* \rightarrow p\pi^0$ it is equal to $-\sqrt{1/3}$. In case of Δ photoproduction, the respective isotopic coefficients are $\sqrt{1/3}$ for $n\pi^+$ and $\sqrt{2/3}$ for $p\pi^0$.

Differential cross sections for $\gamma p \rightarrow n\pi^+$ [17] and PWA result are compared in Fig. 5. In addition to resonances,

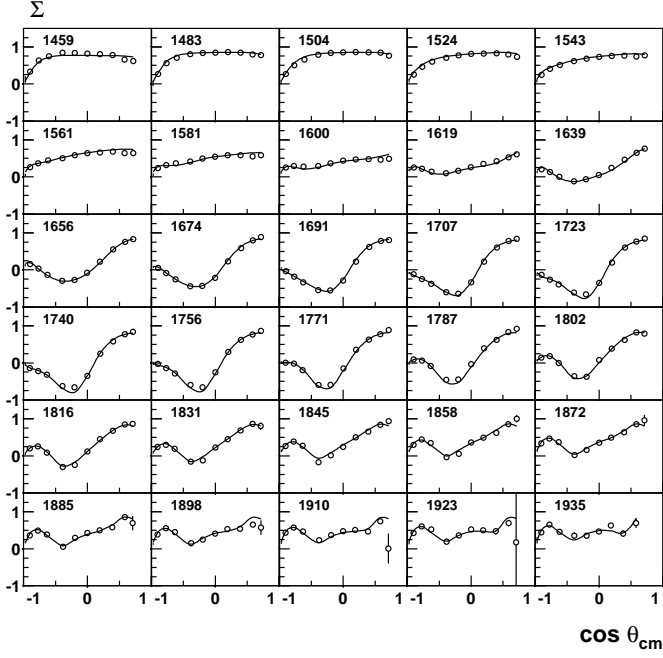


Fig. 3. Photon beam asymmetry Σ for $\gamma p \rightarrow p\pi^0$ from GRAAL [15] and PWA result (solid line).

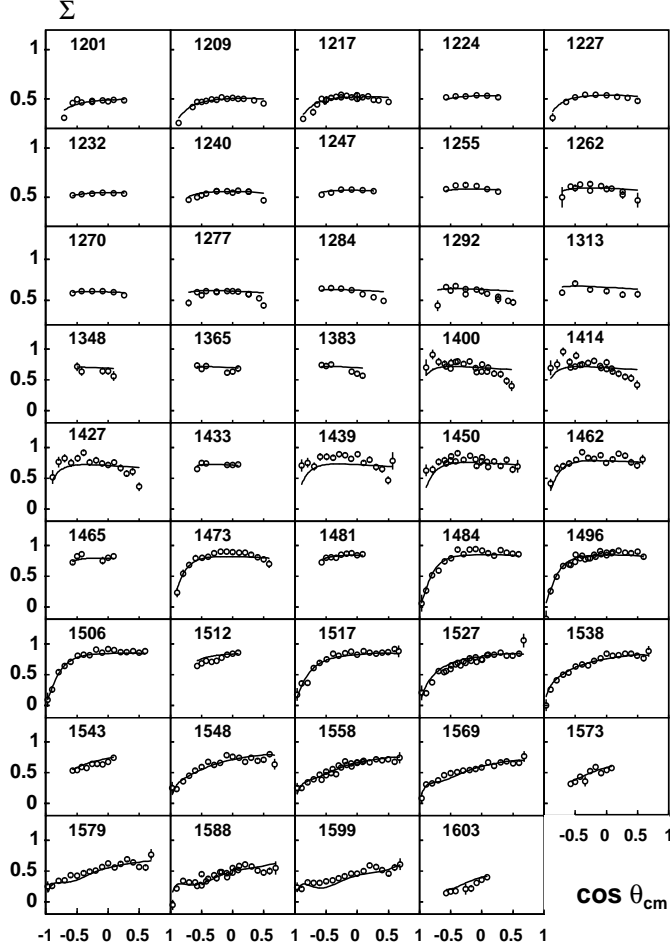


Fig. 4. Photon beam asymmetry Σ for $\gamma p \rightarrow p\pi^0$ from [16] and PWA result (solid line).

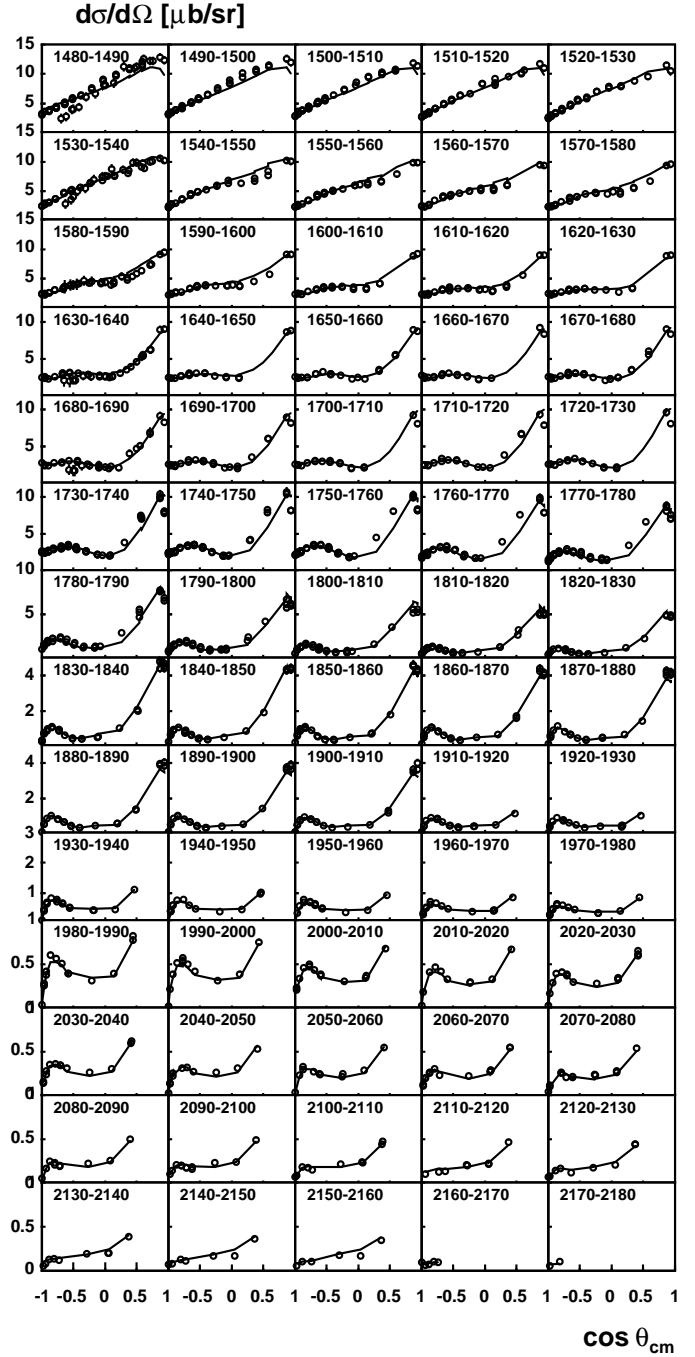


Fig. 5. Differential cross section for $\gamma p \rightarrow n\pi^+$ from [17] and PWA result (solid line).

a significant contribution stems from t -channel π and ρ exchanges (about 10% and 30%, respectively). This reaction has a large number of data points with small statistical errors but the largest ambiguities in its interpretation. Hence, a small weight is given to this channel to avoid that it has a significant impact on baryon masses, widths, or coupling constants. It was only used to stabilise the fits in case of isospin ambiguities.

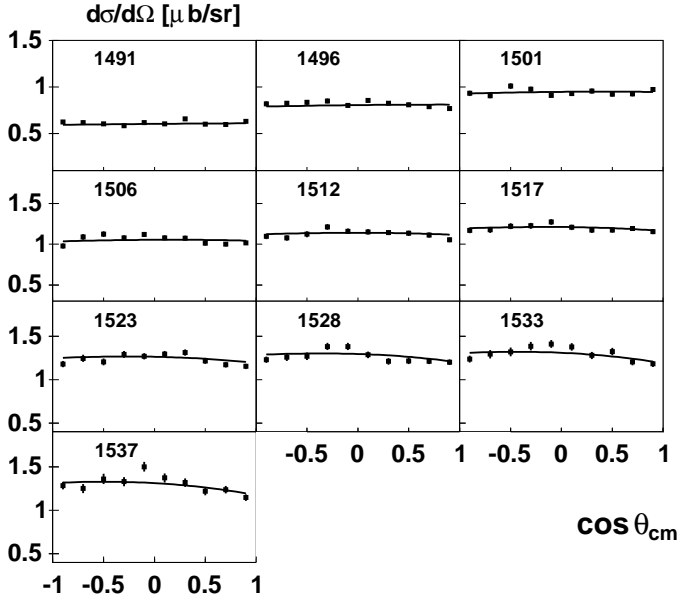


Fig. 6. Differential cross section for $\gamma p \rightarrow p\eta$ from Mainz-TAPS data [18] and PWA result (solid line).

3.3 Fit to the $p\eta$ channel

Differential cross section for $\gamma p \rightarrow p\eta$ in the threshold region were measured by the TAPS collaboration at MAINZ [18]. Data and fit are shown in Fig. 6. In the threshold region, the dominant contribution comes from the $N(1535) S_{11}$ resonance which gives a flat angular distribution. This resonance strongly overlaps with $N(1650) S_{11}$, and a two-pole K-matrix parameterisation is used in the fit.

The CB-ELSA differential cross section [19] is given in Fig. 7 and compared to the PWA results. The contribution of the two S_{11} resonances (dashed line, below 2 GeV) dominates the η production region up to 1650 MeV. The most significant further contributions stem from production of $N(1720) P_{13}$ (dotted line, below 2 GeV), of $N(2070) D_{15}$ (dashed line, above 2 GeV) and $\rho(\omega)$ exchanges (dotted line, above 2 GeV).

Data on the photon beam asymmetry Σ for $\gamma p \rightarrow p\eta$, measured by GRAAL [15] are shown in Fig. 8. This data provides essential information on baryon resonances even if their $(p\gamma)$ - and/or $(p\eta)$ -couplings are weak. In addition, the beam asymmetry data are necessary to determine the ratio of helicity amplitudes.

4 Results

4.1 Total cross sections

From the differential cross sections presented in Figs. 1 and 7, absolute cross sections were determined by integration. The integration is performed by summation of the differential cross sections (dots with error bars) and using extrapolated values for bins with no data, and by integration of the fit curve.

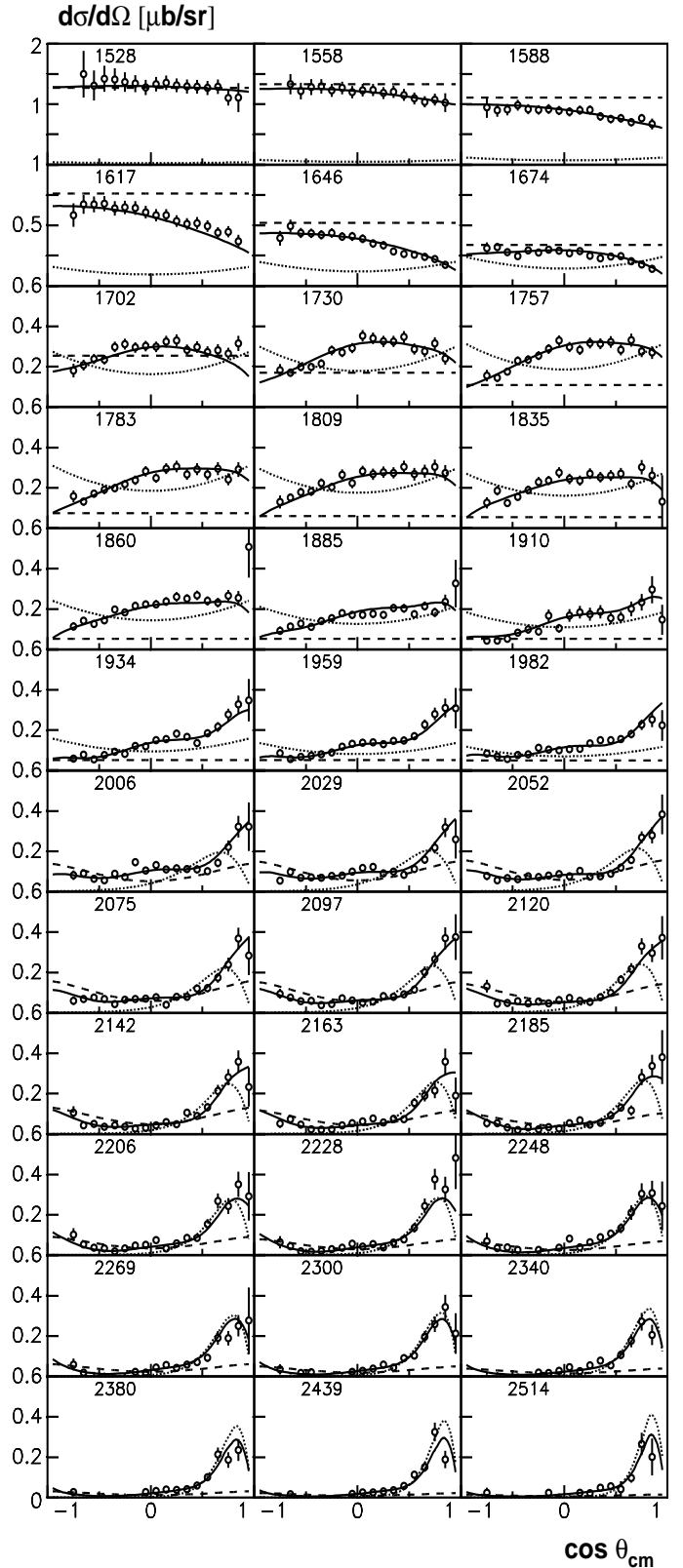


Fig. 7. Differential cross section for $\gamma p \rightarrow p\eta$ from CB-ELSA and PWA result (solid line) [19]. In the mass range below 2 GeV the contribution of the two S_{11} resonances is shown as dashed line and of $N(1720) P_{13}$ as dotted line. Above 2 GeV the contributions of $N(2070) D_{15}$ (dashed line) and $\rho(\omega)$ exchange (dotted line) are shown.

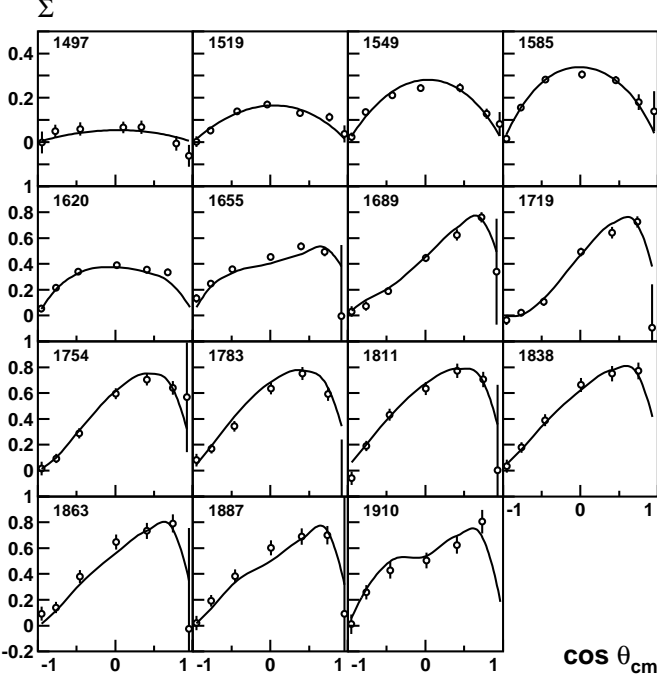


Fig. 8. Photon beam asymmetry Σ for $\gamma p \rightarrow p\eta$ from GRAAL [20] and PWA result (solid line).

In the total cross section for π^0 photoproduction in Fig. 9, clear peaks are observed for the first, second, and third resonance region. With some good will, the fourth resonance region can be identified as broad enhancement at about 1900 MeV. The decomposition of the peaks into partial waves and their physical significance will be discussed below.

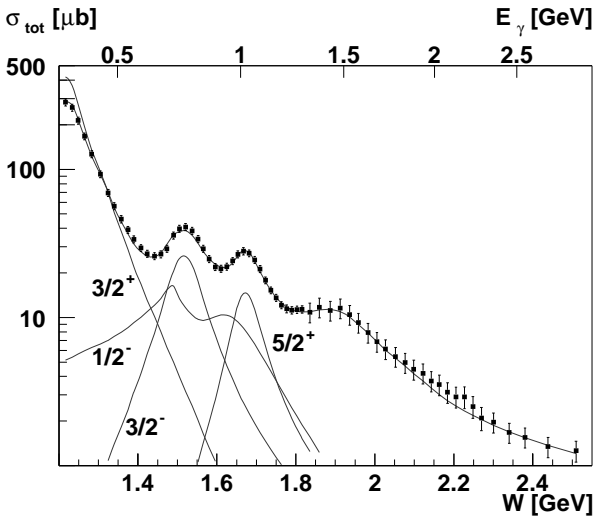


Fig. 9. Total cross section (logarithmic scale) for the reaction $\gamma p \rightarrow p\pi^0$ obtained by integration of angular distributions of the CB-ELSA data and extrapolation into forward and backward regions using our PWA result. The solid line represents the result of the PWA.

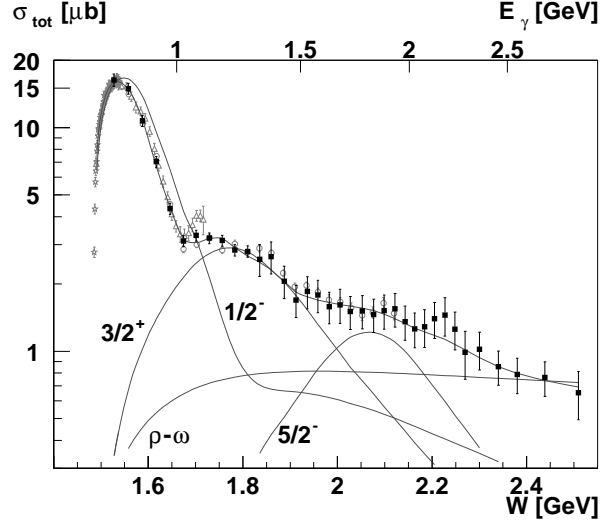


Fig. 10. Total cross section (logarithmic scale) for the reaction $\gamma p \rightarrow p\eta$ [19]. Data from other experiments are shown in grey. The black squares represent the summation over the angular bins (bins not covered by measurements are taken from the fit), the solid line represents our fit. The errors are dominantly due to uncertainties in the normalization. The contributions of the two S_{11} resonances, of $N(1720)P_{13}$, of $N(2070)D_{15}$, and of the background amplitudes (mainly $\rho(\omega)$ exchange) are shown as well.

The η photoproduction cross section (Fig. 10) shows the known strong peak at threshold due to the $S_{11}(1535)$. The cross section exhibits indications for one further resonance below 1800 MeV.

4.2 The best solution

The masses and widths of the observed states are presented in Table 2. Additionally, ratios of helicity amplitudes $A_{1/2}/A_{3/2}$ and fractional contributions normalised to the total cross section for the CB-ELSA π^0 - and η -photoproduction data are included.

A large number of fits (explorative fits plus more than 1000 documented fits) were performed to validate the solution. In these fits the number of resonances, their spin and parity, their parameterisation, and the relative weight of the different data sets were changed.

The errors are estimated from a sequence of fits in which one variable, e.g. a width of one resonance was changed to series of fixed values. All other variables were allowed to adjust freely; the χ^2 changes were monitored as a function of this variable. The errors given in Table 2 correspond to χ^2 changes of 9, hence to three standard deviations. However, the 3σ interval corresponds better to the systematic changes observed when changing the fit hypothesis.

The resonance properties are compared to PDG values [25]. Most resonance parameters converge in the fits to values compatible with previous findings within a 2σ interval of the combined error. The helicity ratios sometimes seem to be inconsistent, however they have large errors and the discrepancies are not really significant.

Three new resonances are necessary to describe the data, $N(1875)D_{13}$, $N(2070)D_{15}$ and $N(2200)$ with uncertain spin and parity. The best fit is achieved for P_{13} quantum numbers. Two further resonances, $N(1840)P_{11}$ and $N(2170)D_{13}$, have masses which are not consistent with established resonances listed by the PDG. We list them also as new particles. Two resonances, $N(2000)F_{15}$ and $\Delta(1940)D_{33}$, are observed for the first time in photoproduction. PDG mass values for $N(2000)F_{15}$ range from 1882 to 2175 MeV. We find a mass of (1850 ± 25) MeV. Our mass for $\Delta(1940)D_{33}$ is fully compatible with PDG. The $\Delta(1940)D_{33}$ contributes only at a marginal level. The χ^2_{tot} changes by 143 units when this resonance is omitted. The $\Delta(1950)F_{37}$ is observed here at 1893 ± 15 MeV instead of (PDG) 1950 ± 10 MeV.

In this paper we concentrate on the $N(2070)D_{15}$ and $N(2200)$. The $N(1840)P_{11}$, $N(1875)D_{13}$, and $N(2170)D_{13}$ do not significantly contribute to $\gamma p \rightarrow p\pi^0$, $p\eta$ and have large couplings to $K\Lambda$ and/or $K\Sigma$. They will be discussed in [8].

Finally a comment is made on resonances with known photo-couplings but not seen in this analysis. $N(1990)F_{17}$, $\Delta(1600)P_{33}$, $\Delta(1910)P_{33}$, $\Delta(1930)D_{35}$, $\Delta(2420)H_{311}$, and $N(2190)G_{17}$ are not observed here. The latter resonance may however be misinterpreted as $N(2200)P_{13}$ (see Table 3). The photocouplings of most of these resonances are seen with weak evidence (one-star rating); only $\Delta(1600)P_{33}$ has a three-star photo-coupling, and the $\Delta(1930)D_{35}$ photocoupling has 2 stars. We have no explanation why these states are missing in this analysis. The $\Delta(1900)S_{31}$, $\Delta(1940)D_{33}$, and $\Delta(1930)D_{35}$ may form a spin triplet with intrinsic orbital angular momentum $L = 1$ and total spin $S = 3/2$ coupling to $J = 1/2, 3/2$, and $5/2$ as suggested in [26]. Two of these states are not observed in this analysis. Quark models do not reproduce these states predicting them to have masses above 2.1 GeV. Hence, the question remains open if these states exist at such a low mass.

4.3 Significance of resonance contributions

A systematic study of the significance of new resonances was carried out. For new resonances the quantum numbers were changed to any J^P value with $J \leq 9/2$. In the new fits, all variables were left free for variations including masses, widths, and couplings of all resonances. The result of this study is summarised in Table 3. The Table illustrates the global deterioration of the fit and the χ^2 changes for the individual channels. Negative χ^2 changes indicate that the best quantum numbers are enforced by other data.

The $N(2070)D_{15}$ is the most significant new resonance. Omitting it changes χ^2_{tot} by 1589, by 199 for the data on η photoproduction and by 940 for the data on π^0 photoproduction. Replacing the J^P assignment from $5/2^-$ to $1/2^\pm$, ..., $9/2^\pm$, the χ^2_{tot} deteriorates by more than 750. The deterioration of the fits is visible in the comparison of data and fit. One of the closest description for η photoproduction was obtained fitting with a $7/2^-$ state. In this case, Figs. 11 a,b show the fits of the differential cross

Table 3. Changes in χ^2 when one of the new resonances is omitted or replaced by a resonance with different spin and parity J^P . The changes are given for the χ^2_{tot} (13) and the χ^2 contributions for individual final states calculated analogously.

Resonance	N(2070)D ₁₅				
J^P	$\Delta\chi^2_{\text{tot}}$	$\Delta\chi^2_{p\pi^0}$	$\Delta\chi^2_{p\eta}$	$\Delta\chi^2_{\Lambda K^+}$	$\Delta\chi^2_{\Sigma K}$
omitted	1588	940	199	94	269
repl. by $1/2^-$	1027	669	128	111	-45
repl. by $3/2^-$	1496	851	214	-46	157
repl. by $7/2^-$	1024	765	108	-1	19
repl. by $9/2^-$	872	656	112	-9	118
repl. by $1/2^+$	832	674	115	55	33
repl. by $3/2^+$	1050	690	141	-42	20
repl. by $5/2^+$	766	627	113	48	123
repl. by $7/2^+$	807	718	112	-67	215
repl. by $9/2^+$	1129	847	131	7	-9

Resonance	N(2200)P ₁₃				
J^P	$\Delta\chi^2_{\text{tot}}$	$\Delta\chi^2_{p\pi^0}$	$\Delta\chi^2_{p\eta}$	$\Delta\chi^2_{\Lambda K^+}$	$\Delta\chi^2_{\Sigma K}$
omitted	190	1	37	43	20
repl. by $1/2^-$	46	-18	10	40	0
repl. by $7/2^-$	10	-10	7	23	17
repl. by $9/2^-$	18	-82	8	16	16
repl. by $1/2^+$	50	-8	9	26	42
repl. by $5/2^+$	17	-15	10	21	5
repl. by $7/2^+$	13	-13	13	-10	18
repl. by $9/2^+$	19	-9	5	14	17

section in the region of resonance mass and description of the beam asymmetry for highest energy bin. The shape of the differential cross section at small angles is close in both cases however the $7/2^-$ state failed to describe the very forward two points. The beam asymmetry also clearly favours the $5/2^-$ state. The π^0 photoproduction cross sections measured by CB-ELSA are visually not too sensitive to $5/2^-$ and $7/2^-$ quantum numbers (see Fig. 11 c) but there is a clear difference between the two descriptions in the very backward region. The latest GRAAL results on the $p\pi^0$ differential cross section which were obtained after discovery of the $N(2070)D_{15}$ [14] confirmed $5/2^-$ as favoured quantum numbers (see Fig. 11 d).

The mass scan of the $D_{15}(2070)$ resonance (χ^2 as a function of the assumed D_{15} mass) is shown in Fig. 12. In the scan, the mass of the D_{15} was fixed at a number of values covering the region of interest while all other fit parameters were allowed to adjust newly. The sum of χ^2 for π^0 photoproduction data (CB-ELSA, GRAAL 05) does not show any minimum in this region; the distributions are very flat. Fig. 12a shows separately the sum of χ^2 contributions from the CB-ELSA differential cross section plus the GRAAL 04 polarisation data, and the sum of the χ^2 for all ΛK^+ and all ΣK reactions. A clear minimum is seen in all three data sets. The sum of χ^2 for all these reactions is given in Fig. 12b. The shaded area corresponds to the mass range assigned to this resonance, (2060 ± 30) MeV. We conclude that the $D_{15}(2070)$ is iden-

Table 2. Masses, widths and helicity ratio, this analysis.

Resonance	M (MeV)	Γ (MeV)	$A_{1/2}/A_{3/2}$	Fraction $\gamma p \rightarrow p\eta$	Fraction $\gamma p \rightarrow p\pi^0$	PDG Rating overall	N γ
N(1440)P ₁₁	1450 \pm 50	250 \pm 150			0.007		
PDG	1440 ⁺³⁰ ₋₁₀	350 \pm 100				****	***
N(1520)D ₁₃	1526 \pm 4	112 \pm 10	-0.02 \pm 0.10	0.030	0.140		
PDG	1520 ⁺¹⁰ ₋₅	120 ⁺¹⁵ ₋₁₀	-0.14 \pm 0.06			****	****
N(1535)S ₁₁ *	1530 \pm 30	210 \pm 30					
PDG	1505 \pm 10	170 \pm 80		0.830	0.170	****	***
N(1650)S ₁₁ *	1705 \pm 30	220 \pm 30					
PDG	1660 \pm 20	160 \pm 10				***	****
N(1675)D ₁₅	1670 \pm 20	140 \pm 40	0.40 \pm 0.25	0.002	0.001		
PDG	1675 ⁺¹⁰ ₋₅	150 ⁺³⁰ ₋₁₀	1.27 \pm 0.93			****	****
N(1680)F ₁₅	1667 \pm 6	102 \pm 15	-0.13 \pm 0.05	0.005	0.069		
PDG	1680 ⁺¹⁰ ₋₅	130 \pm 10	-0.11 \pm 0.05			****	****
N(1700)D ₁₃	1725 \pm 15	100 \pm 15	0.45 \pm 0.25	0.044	0.002		
PDG	1700 \pm 50	100 \pm 50	9.00 \pm 6.5			***	**
N(1720)P ₁₃	1750 \pm 40	380 \pm 40	1.5 \pm 1.1	0.400	0.016		
PDG	1720 ⁺³⁰ ₋₇₀	250 \pm 50	-0.9 \pm 1.8			***	**
N(1840)P ₁₁	1840 ⁺¹⁵ ₋₄₀	140 ⁺³⁰ ₋₁₅		0.029	0.003	new	new
PDG	1720 \pm 30	100 ⁺¹⁵⁰ ₋₅₀				***	***
N(1875)D ₁₃	1875 \pm 25	80 \pm 20	1.20 \pm 0.45	0.013	0.000	new	new
N(2000)F ₁₅	1850 \pm 25	225 \pm 40	0.13 \pm 1.10	0.010	0.004		new
PDG	\sim 2000					**	
N(2070)D ₁₅	2060 \pm 30	340 \pm 50	1.10 \pm 0.30	0.195	0.012	new	new
N(2170)D ₁₃	2166 ⁺²⁵ ₋₅₀	300 \pm 65	-1.40 \pm 0.80	0.003	0.002	new	new
PDG	\sim 2080					**	*
N(2200)P ₁₃	2200 \pm 30	190 \pm 50	-0.35 \pm 0.40	0.015	0.000	new	new
$\Delta(1232)P_{33}^\diamond$	1235 \pm 4	140 \pm 12	0.44 \pm 0.06		0.709		
PDG	1232 \pm 2	120 \pm 5	0.53 \pm 0.04			****	****
$\Delta(1620)S_{31}$	1635 \pm 6	106 \pm 12			0.023		
PDG	1620 ⁺⁵⁵ ₋₅	150 \pm 30				****	***
$\Delta(1700)D_{33}$	1715 \pm 20	240 \pm 35	1.15 \pm 0.25		0.056		
PDG	1700 ⁺⁷⁰ ₋₃₀	300 \pm 100	1.2 ^{+0.6} _{-0.4}			****	***
$\Delta(1905)F_{35}$	1870 \pm 50	370 \pm 110	> 10		0.001		
PDG	1905 ⁺¹⁵ ₋₃₅	350 ⁺⁹⁰ ₋₇₀	-0.6 ^{+0.4} _{-0.9}			****	***
$\Delta(1920)P_{33}$	1996 \pm 30	380 \pm 40	0.45 \pm 0.20		0.050		
PDG	1920 ⁺⁵⁰ ₋₂₀	200 ⁺¹⁰⁰ ₋₅₀	1.7 ⁺⁷ _{-1.0}			****	*
$\Delta(1940)D_{33}$	1930 \pm 40	200 \pm 100	0.20 \pm 0.40		0.010		new
PDG	\sim 1940					*	
$\Delta(1950)F_{37}$	1893 \pm 15	240 \pm 30	0.75 \pm 0.11		0.027		
PDG	1950 \pm 10	300 ⁺⁵⁰ ₋₁₀	0.8 \pm 0.2			****	****

* K -matrix fit, pole position of the scattering amplitude in the complex plane, fraction for the total K -matrix contribution

\diamond This contribution includes non-resonant background.

tified in its decays into $N\eta$, ΛK^+ and ΣK . Its coupling to $N\pi$ is weak, hence it is not surprising that it was not observed in pion induced reactions.

The $N(2200)$ resonance is less significant. Omitting $N(2200)$ from the analysis, changes χ^2 for the CB-ELSA data on η photoproduction by 56, and by 20 for the π^0 -photoproduction data. Other quantum numbers than the preferred P_{13} lead to marginally larger χ^2 values. The mass scan for this state is shown in Fig. 13. The photoproduction data on $d\sigma/d\Omega$ from CB-ELSA does not show any minimum, η photoproduction data exhibit a shallow minimum slightly above 2200 MeV. The sum of all ΛK^+ and $K\Sigma$ reactions also have a minimum in this mass region. The sum of χ^2 for all these reactions is shown in

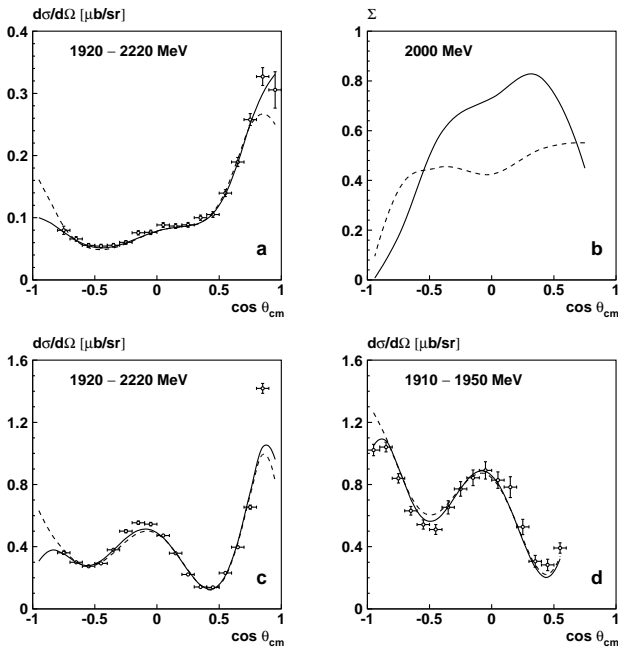


Fig. 11. Differential cross section (a), beam asymmetry (b, predicted curves) from the reaction $\gamma p \rightarrow p\eta$ and differential cross sections for π^0 photoproduction from CB-ELSA (c) and GRAAL05 (d). Our best PWA fit with $N(2070)D_{15}$ is shown as solid line, the dotted line shows a fit when the $5/2^-$ resonance is replaced by a $7/2^-$ state.

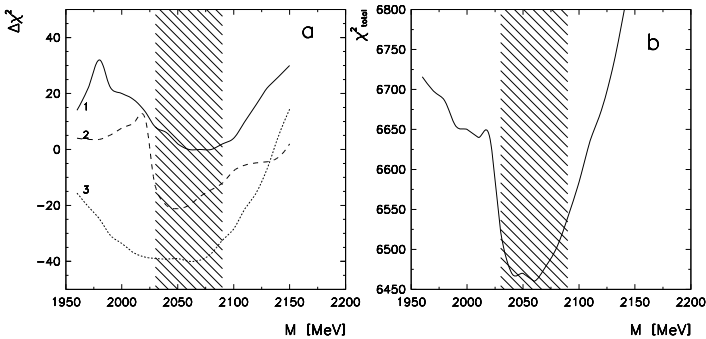


Fig. 12. The result of $D_{15}(2070)$ mass scan: a) 1 – $d\sigma/d\Omega$ for $\gamma p \rightarrow p\eta$ (CB-ELSA), 2 – sum of all reactions with ΛK^+ final state multiplied with $1/5$, 3 – sum of all reactions with ΣK final state multiplied with $1/5$, b) the total χ^2 for all reactions shown in a).

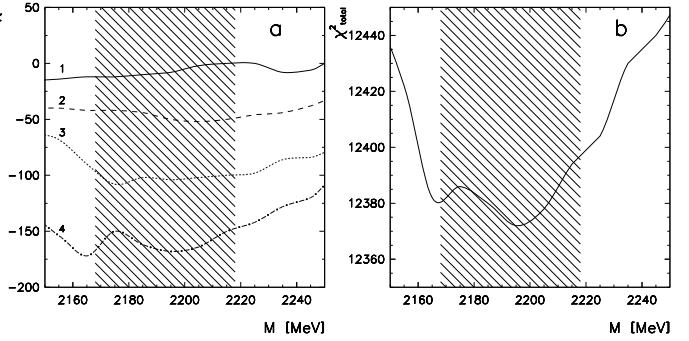


Fig. 13. The result of $P_{13}(2200)$ mass scan: a) 1 – $d\sigma/d\Omega$ for $\gamma p \rightarrow p\pi^0$ (CB-ELSA), 2 – $d\sigma/d\Omega$ for $\gamma p \rightarrow p\eta$ (CB-ELSA), 3 – sum of all reactions with ΛK^+ final state 4 – sum of all reactions with ΣK final state b) the total χ^2 for all reactions shown in a).

Fig. 13 b) and from this distribution the resonance mass can be well defined.

4.4 The four resonance regions

The first resonance region dominates pion photoproduction and is due to the excitation of the $\Delta(1232)P_{33}$. Its fractional contribution to $\gamma p \rightarrow p\pi^0$ (Table 2) exceeds 1. There is strong destructive interference between $\Delta(1232)P_{33}$, the P_{33} nonresonant amplitude and u -channel exchange. In the fit without latest GRAAL data on the cross section and beam asymmetry [15] the $A_{1/2}/A_{3/2}$ helicity ratio of excitation of the $\Delta(1232)P_{33}$ was found to be 0.52 ± 0.06 which agrees favorably with the PDG average 0.53 ± 0.04 . With the new GRAAL05 data included, this value shifted to 0.44 ± 0.06 . The $N(1440)P_{11}$ Roper resonance provides a small contribution of about 1–3% compared to the $\Delta(1232)P_{33}$.

In the $p\pi^0$ final state $N(1520)D_{13}$ and the two S_{11} resonances yield contributions of similar strengths to the second resonance region. This is consistent with the known photocouplings and $p\pi$ branching fractions of the three resonances.

The third bump in the $p\pi^0$ total cross section is due to three major contributions: the $\Delta(1700)D_{33}$ resonance provides the largest fraction ($\sim 35\%$) of the peak, followed by $N(1680)F_{15}$ ($\sim 25\%$) and $N(1650)S_{11}$ ($\sim 20\%$) as extracted from the K -matrix parameterisation; observed as well are the $\Delta(1620)S_{31}$ ($\sim 7\%$) and $N(1720)P_{13}$ ($\sim 6\%$) resonances. The latter contributes to $p\eta$ with a surprisingly large fraction; about 90% of the resonant intensity in this mass region is assigned to $N(1720)P_{13} \rightarrow p\eta$ decays.

In the fourth resonance region we identify $\Delta(1950)F_{37}$ contributing $\sim 41\%$ to the enhancement and $\Delta(1920)P_{33}$ with $\sim 35\%$. Additionally, the fit requires the presence of $\Delta(1905)F_{35}$ and $\Delta(1940)D_{33}$. The high-energy region is dominated by $\rho(\omega)$ exchange in the t channel as can be seen by the forward peaking in the differential cross sections.

4.5 Discussion

Four new resonances are found in this analysis. The question arises of course why these resonances have not been found before. $N(2070)D_{15}$ has a large coupling to $N\eta$ and may therefore have escaped discovery. The $N(1875)D_{13}$ and $N(2170)D_{13}$ states couple strongly to the $K\Lambda$ and $K\Sigma$ channels; the existence of the first state has already been suggested in [27] from an analysis of older SAPHIR data on $\gamma p \rightarrow K\Lambda$ [28]. Cutkosky [29] reported two $N D_{13}$ resonances at (1880 ± 100) and (2081 ± 80) MeV with respective widths of (180 ± 60) and (300 ± 100) MeV. The $N(1840)P_{11}$ appears in all channels. The evidence for it is discussed in [8]. The $N(2200)$ does not have such characteristic features. It improves the description of the data in a difficult mass range and further data will be required to establish or to disprove its existence. Its preferred quantum numbers are P_{13} but it seems not unlikely that $N(2200)$ should be identified with $N(2190)G_{17}$ (which gives the second best PWA solution).

The three largest contributions to the η photoproduction cross section stem from $N(1535)S_{11}$, $N(1720)P_{13}$, and $N(2070)D_{15}$. We tentatively assign $(J = 1/2; L = 1, S = 1/2)$ quantum numbers to the first state; $N(1720)P_{13}$ and $N(1680)F_{15}$ form a spin doublet, hence the dominant quantum numbers of $N(1720)P_{13}$ must be $(J = 3/2; L = 2, S = 1/2)$. Thus it is tempting to assign $(J = 5/2; L = 3, S = 1/2)$ quantum numbers to $N(2070)D_{15}$. The three baryon resonances with strong contributions to the $p\eta$ channel thus all have spin $S = 1/2$ and orbital and spin angular momenta adding antiparallely with $J = L - 1/2$. Fig. 14 depicts this scenario.

The large $N(1535)S_{11} \rightarrow N\eta$ coupling has been a topic of a controversial discussion. In the quark model, this coupling arises naturally from a mixing of the two $(J = 1/2; L = 1, S = 1/2)$ and $(J = 1/2; L = 1, S = 3/2)$ harmonic-oscillator states [30]. However, $N(1535)S_{11}$ is very close to the $K\Lambda$ and $K\Sigma$ thresholds and the resonance can be understood as originating from coupled-channel meson-

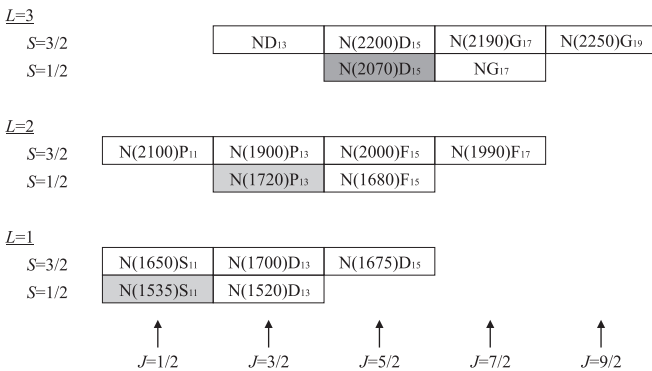


Fig. 14. N^* resonances with quantum numbers which can be assigned to orbital angular momentum excitations with $L = 1, 2, 3$. The quark spin, $S = 1/2$ or $S = 3/2$, and the orbital angular momentum couple to the total spin J . Note that mixing between states of the same parity and total angular momentum is possible. Resonances with strong coupling to the $N\eta$ channel are marked in grey.

baryon chiral dynamics [31]. Alternatively, the strong $N(1535)S_{11} \rightarrow N\eta$ coupling can be explained as delicate interplay between confining and fine structure interactions [32].

A consistent picture of the large $N(1535)S_{11} \rightarrow N\eta$ coupling should explain the systematics of $N\eta$ couplings. We note a kinematical similarity: The three resonances with large $N\eta$ partial decay widths are those for which the dominant intrinsic orbital excitation $L = 1, 2, 3$ and the decay orbital angular momenta $\ell = 0, 1, 2$ are related by $J = L - 1/2 = \ell + 1/2$. The intrinsic quark spin configuration remains in a spin doublet.

5 Summary

We have presented a partial wave analysis of data on photoproduction of πN , ηN , $K\Lambda$, and $K\Sigma$ final states. The data include total cross sections and angular distributions, beam asymmetry measurements as well as the recoil polarisation in case of hyperon production. A reasonable description of all data was achieved by introducing 14 N^* and seven Δ^* resonances.

Most baryon resonances are found with masses, widths and ratios of helicity amplitudes which are fully compatible with previous findings. New resonances are required to fit the data, $N(1840)P_{11}$, $N(1875)D_{13}$, $N(2070)D_{15}$, $N(2170)D_{13}$, and $N(2200)$. The $N(1840)P_{11}$ resonance could, however, be identical with $N(1710)P_{11}$ and $N(2170)D_{13}$ with $N(2080)D_{13}$.

Three resonances are found to have very large couplings to $N\eta$, $N(1535)S_{11}$, $N(1720)P_{13}$, and $N(2070)D_{15}$. The dynamical origin of this preference remains to be investigated.

Acknowledgements

We would like to thank the CB-ELSA/TAPS Collaboration for numerous discussions on topics related to this work. We acknowledge financial support from the Deutsche Forschungsgemeinschaft within the SFB/TR16. The collaboration with St.Petersburg received funds from the DFG and the Russian Foundation for Basic Research. U. Thoma thanks for an Emmy Noether grant from the DFG. A.V. Anisovich and A.V. Sarantsev acknowledge support from the Alexander von Humboldt Foundation.

References

1. N. Isgur, "Baryons: The promise, the problems, and the prospects", *7th International Conference on the Structure of Baryons*, (B.F. Gibson et al. eds.), Santa Fe, New Mexico, 3-7 Oct 1995, World Scientific, Singapore, 1996.
2. S. Capstick and N. Isgur, Phys. Rev. D **34** (1986) 2809.
S. Capstick and W. Roberts, Prog. Part. Nucl. Phys. **45** (2000) S241.
3. L. Y. Glozman, W. Plessas, K. Varga, and R. F. Wagenbrunn, Phys. Rev. D **58** (1998) 094030.

4. U. Löring, K. Kretzschmar, B. C. Metsch, and H. R. Petry, Eur. Phys. J. A **10** (2001) 309.
U. Löring, B. C. Metsch, and H. R. Petry, Eur. Phys. J. A **10** (2001) 395, 447.
5. E. Klempt, “Glueballs, hybrids, pentaquarks: Introduction to hadron spectroscopy and review of selected topics”, arXiv:hep-ph/0404270, and refs. therein.
6. A. R. Dzierba, C. A. Meyer, and A. P. Szczepaniak, “Reviewing the evidence for pentaquarks”, arXiv:hep-ex/0412077.
7. K. Hicks, “Experimental search for pentaquarks”, arXiv:hep-ex/0504027.
8. A. Sarantsev *et al.*, “Decays of Baryon Resonances into ΛK^+ , $\Sigma^0 K^+$ and $\Sigma^+ K^0$ ”, subsequent paper.
9. G. Veneziano, Phys. Rep. **9C** (1973) 199.
10. M.A.Polyakov and V.V.Vereshchagin, Eur.Phys.J **A12** (2001) 349.
11. V. V. Anisovich, D. V. Bugg, A. V. Sarantsev, and B. S. Zou, Phys. Atom. Nucl. **57** (1994) 1595 [Yad. Fiz. **57** (1994) 1666].
12. A. Anisovich, E. Klempt, A. Sarantsev, and U. Thoma, Eur. Phys. J. A **24** (2005) 111.
13. P.D.B. Collins and E.J.Squires, “An introduction to Regge theory and high energy physics”, Cambridge U.P., 1976.
14. O. Bartholomy *et al.*, Phys. Rev. Lett. **94** (2005) 012003.
15. GRAAL collaboration, article in preparation. We thank the GRAAL collaboration for providing their (preliminary) data to us prior to publication.
16. A. A. Belyaev *et al.*, Nucl. Phys. B **213** (1983) 201.
R. Beck *et al.*, Phys. Rev. Lett. **78** (1997) 606.
D. Rebreyend *et al.*, Nucl. Phys. A **663** (2000) 436.
17. K. H. Althoff *et al.*, Z. Phys. C **18** (1983) 199.
E. J. Durwen, BONN-IR-80-7 (1980).
K. Buechler *et al.*, Nucl. Phys. A **570** (1994) 580.
18. B. Krusche *et al.*, Phys. Rev. Lett. **74** (1995) 3736.
19. V. Crede *et al.*, Phys. Rev. Lett. **94** (2005) 012004.
20. J. Ajaka *et al.*, Phys. Rev. Lett. **81** (1998) 1797.
21. K. H. Glander *et al.*, Eur. Phys. J. A **19** (2004) 251.
22. J. W. C. McNabb *et al.*, Phys. Rev. C **69** (2004) 042201.
23. R. G. T. Zegers *et al.*, Phys. Rev. Lett. **91** (2003) 092001.
24. R. Lawall *et al.*, “Measurement of the reaction $\gamma p \rightarrow K^0 \Sigma^+$ at photon energies up to 2.6 GeV”, arXiv:nucl-ex/0504014.
25. S. Eidelman *et al.*, Phys. Lett. B **592** (2004) 1.
26. E. Klempt, “Baryon resonances and strong QCD”, arXiv:nucl-ex/0203002,
E. Klempt, Phys. Rev. C **66** (2002) 058201.
27. T. Mart and C. Bennhold, Phys. Rev. C **61** (2000) 012201.
28. M. Q. Tran *et al.*, Phys. Lett. B **445** (1998) 20.
29. R. E. Cutkosky, C. P. Forsyth, J. B. Babcock, R. L. Kelly, and R. E. Hendrick, “Pion - Nucleon Partial Wave Analysis”, *4th Int. Conf. on Baryon Resonances, Toronto, Canada, Jul 14-16, 1980*, in: Baryon 1980, QCD191 **C45** 1980.
30. N. Isgur and G. Karl, Phys. Rev. D **18** (1978) 4187.
31. N. Kaiser, P. B. Siegel, and W. Weise, Phys. Lett. B **362** (1995) 23.
32. L. Y. Glozman and D. O. Riska, Phys. Lett. B **366** (1996) 305.

